Nuclear Instruments and Methods in Physics Research A 491 (2002) 41–53

NUCLEAR INSTRUMENTS & METHODS IN PHYSICS RESEARCH
Section A

www.elsevier.com/locate/nima

The time-of-flight detector of the DIRAC experiment ☆

B. Adeva, M.V. Gallas, F. Gómez, A. López-Agüera, T. Núñez-Pardo, M. Pló, A.M. Rodríguez*, X.M. Rodríguez, J.J. Saborido, C. Santamarina, M.J. Tobar, P. Vázquez

Departamento de Física de Partículas, Universidade de Santiago de Compostela, Santiago 15782, Spain

Received 22 January 2002; received in revised form 29 April 2002; accepted 11 May 2002

Abstract

The construction and performance of a large area time-of-flight detector for the DIRAC experiment at CERN is reported. With an average time resolution of 123 ps per counter at rates up to 1 MHz, it allows excellent separation of $p\pi^-$ from $\pi^+\pi^-$ pairs up to 4.6 GeV/c momentum, as well as of Coulomb-correlated pion pairs from accidentals. The optimization of scintillator material, photomultiplier performance and readout electronics is described. © 2002 Elsevier Science B.V. All rights reserved.

PACS: 29.40.Mc; 85.60.Ha; 29.90.Tr

Keywords: DIRAC; Time of flight; Plastic scintillator; Particle identification

1. Overview of the DIRAC experiment

The DIRAC experiment at CERN aims to form Pionium ($\pi^+\pi^-$ atomic states) and to measure its lifetime with 10% accuracy [1]. The method for detecting such $\pi^+\pi^-$ Coulomb bound states is to produce them by means of a high intensity proton beam colliding on a thin nuclear target, and to observe $\pi^+\pi^-$ pairs from the atom break-up (ionization) within the target. These "atomic pairs" are characterized by the low relative momentum Q in their center of mass system ($Q < 3$ MeV/c) and they are identified as an excess over the background of free pion pairs. The DIRAC experimental setup was then designed to detect charged pion pairs at small opening angle with very high momentum resolution, both in the longitudinal and transverse components (better than 1 MeV/c for Q_L and 0.5 MeV/c for Q_T).

It consists of a double arm magnetic spectrometer which was installed and commissioned in 1998 at the T8 beam area of the PS East Hall at CERN. The spectrometer is arranged on a secondary particle channel, inclined upwards by 5.7° with respect to the incoming proton beam direction, and the channel aperture is 1.2 m sr. The 24 GeV/c beam is delivered in the form of 0.40 s spills with 1×10^{11} protons, that impinges on the DIRAC nuclear target station. To track the

---

☆Work supported by Ministerio de Ciencia y Tecnologia (MCYT), under projects AEN96-1671 and AEN99-0488, and by Xunta de Galicia, under projects INFRA 96 ED405A and PGIDT00PXI20602PR.

*Corresponding author. Tel.: +34-981-563100-ext. 14012; fax: +34-981-521091.

E-mail address: xose@fpsunae2.usc.es (A.M. Rodríguez).

PII: S0168-9002(02)01121-X

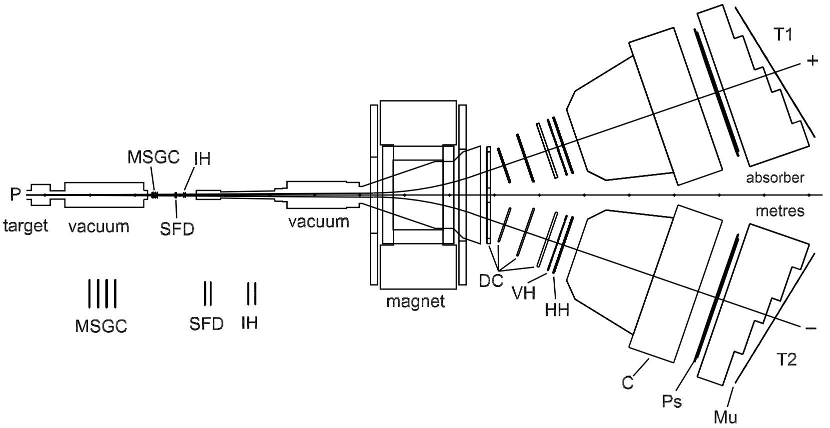

Fig. 1. Top view of the DIRAC spectrometer. The TOF detector is placed downstream the magnet at a distance of 11.6 m form the target.

produced $\pi^+\pi^-$ pairs, a first set of detectors is placed upstream of the spectrometer magnet: four planes of a Gas Electron Multiplier (GEM) with MSGC readout, a Scintillation Fiber Detector (SFD) and an Ionization Hodoscope (IH). The pairs are split up in the horizontal plane by a 1.65 T dipole magnet. Downstream the magnet two identical arms have been built each including the following detectors: a fast Drift Chamber system (DC); the Vertical Hodoscope (VH) array, or time-of-flight (TOF) detector described in this article; a Horizontal Hodoscope; a threshold gas Cherenkov counter (C); a Preshower counter (Ps); a Muon identification system (Mu) [2]. A top view of the DIRAC setup is shown in Fig. 1.

A multi-trigger system is installed to cope with the very high counting rates in the spectrometer and to select small relative momentum pairs ($Q < 30$ MeV/c) [3]. The trigger performance relies heavily on the VH detector described in this paper.

2. Purpose and requirements

In such double-arm spectrometer a hodoscope system is necessary to provide a fast coincidence between the positive and negative arms, at the first level of trigger. This is achieved with the vertical hodoscope array described in this article (called TOF system throughout the text), in conjunction with an additional array of horizontal hodoscopes covering the same acceptance. The latter is used to provide a planarity requirement for the pion pairs [3,2], and will not be described here. The TOF detector in DIRAC is also used in a specific fast trigger algorithm, the so-called level 3 trigger, which selects equal-momentum pairs ($Q < 30$ MeV/c) by means of correlations between this detector and a small vertical hodoscope before the magnet [4].

Besides the performance related to its trigger function, the detector must achieve two additional goals:

- separation in the off-line analysis between real (Coulomb-correlated) and accidental (non-Coulomb-correlated) pion pairs with maximum purity. The latter are required by the experimental procedure in order to perform an accurate calibration of the Coulomb interaction,
- identification of background pairs other than $\pi\pi$, mainly $p\pi^-$, missidentified $e\pi$, and to a lesser extent $K\pi$ pairs.

Within the geometry and momentum coverage of the spectrometer from 1 to 6 GeV/c, the previous two requirements can only be achieved with a resolution in the time difference between the two arms better than 200 ps (141 ps for single measurements). Note that since we actually tag particle pairs, no additional detector is required to perform this measurement. This resolution must be sustained up to a counting rate reaching 1 MHz per counter at maximum.

3. Detector design and optimization

The TOF detector consists in two identical scintillation hodoscopes located downstream the magnet along the secondary particle channel and covering an area of 5040 cm^2 in each spectrometer arm. Each hodoscope includes an array of 18 long rectangular scintillator counters, vertically arranged. An overall picture of this detector after installation can be appreciated in Fig. 3.

In Fig. 2, a scheme of one individual counter is shown. The scintillator material is Bicron BC420 and the slab dimensions are 40 cm length, 7 cm width and 2.2 cm thickness. In order to avoid position dependence in the time measurements, it is read out at both ends by two photomultipliers coupled to a fish-tail light guide.

Let us briefly review the constraints in the design of a detector of this kind, and describe how the scintillation material, photon detector and the readout electronics were optimized to achieve the best resolution.

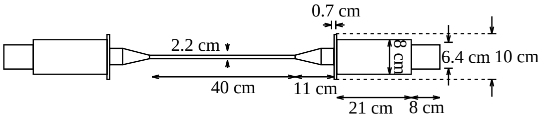

Fig. 2. Lateral view of a TOF counter slab.

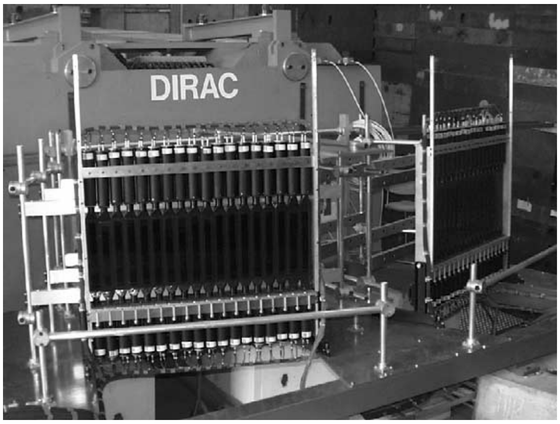

Fig. 3. Photography of the TOF detector during installation in the DIRAC experimental area after the dipole magnet.

The time jitter in a TOF measurement, using scintillation detectors, receives contributions from at least the following sources:

- interaction time with the scintillator and scintillator decay time ($\sigma_{\rm sci}$),
- time spread in the light collection due to path length variations ($\sigma_{\rm pl}$),
- time jitter in the photomultiplier, including transit time spread ($\sigma_{\rm pmt}$),
- time walk in the electronics readout system, including discrimination, mean-timing, digital conversion and delay lines ($\sigma_{\rm el}$).

A simple parametrization of the overall contribution [5] comes from the assumption that the first three sources can be applied to individual photons or photoelectrons, and therefore scale as $1/\sqrt{N_{\rm pe}}$, with $N_{\rm pe}$ being the number of photoelectrons. This is expressed in the very approximate formula:

$$\sigma_t = \sqrt{\frac{\sigma^2_{\rm sci} + \sigma^2_{\rm pm} + \sigma^2_{\rm pl}}{N_{\rm pe}} + \sigma^2_{\rm el}}. \tag{1}$$

We have studied the light output and the resolution characteristics of different scintillator materials, photomultipliers and readout electronics, in a series of tests performed at the T9 beam line of the PS accelerator at CERN. The beam was set to select charged pions with momentum between 1 and 5 GeV/c. The rate capability was tested using different beam intensities, to produce average particle rates ranging from 1×10^4 to 2×10^6 s^{-1}, corresponding to the requirements of the DIRAC experiment. The results are reported in the following subsections.

3.1. Scintillator material

Two main requirements must be fulfilled by the scintillator material, aiming for a good time resolution:

- the characteristic decay time of light emission processes has to be as short as possible,
- the number of photoelectrons that reach the photomultiplier has to be large enough, and

Table 1
Main features of the three scintillator materials chosen as candidates for the construction of the DIRAC TOF detector

Plastic	% light	Rise time (ns)	Decay time (ns)	λ (cm)
Bc408	64	0.9	2.1	210
Bc420	64	0.5	1.5	140
IHEP	56	0.6	1.9	80

independent of the impact point over the counter front dimensions. This implies a high efficiency to convert the ionization energy into scintillation light as well as in photon transmission to the photomultiplier.

Three different materials were considered as possible candidates: BC-408 and BC-420 from BICRON, oriented to ultra-fast timing applications, and a scintillator material developed by the High Energy Physics Institute IHEP in Protvino (Russia) [6,7]. In Table 1, the main features of these plastic materials are summarized.

In the CERN test, the pulse-height resolution was examined for each case, and the light attenuation checked by varying the position of the beam along the counter. We determined the average pulse-height in the ADC ($\langle \mathrm{ADC} \rangle$), and the width of its distribution in a Gaussian fit (σ_{ph}). For those cases in which the pulse-height resolution were fully described by photoelectron statistics, it is known that the squared ratio $(\langle \mathrm{ADC} \rangle / \sigma_{\mathrm{ph}})^2$ determines the number of photoelectrons. However, there are in general other possible fluctuations contributing to this quantity, particularly in the cases where the number of photoelectrons is large. We have empirically taken this ratio as a reference for the relative performance of the counters using different materials. The results are given in Fig. 4 for each scintillator, at three different positions of the beam spot with respect to the light guide. The BC-420 produces the largest values (208 near the light guide), and it also shows better uniformity.

3.2. Photon detection

As explained before, the main requirements for the photomultiplier and the voltage divider are in first place, to provide a detector resolution in the time difference better than 200 ps, and secondly to guaranty a stable operation at high particle rates, up to 1 MHz.

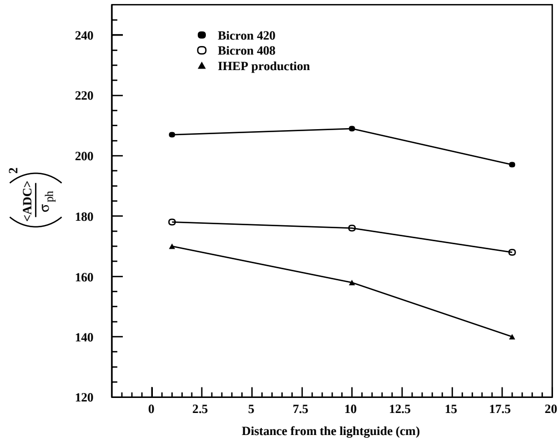

Fig. 4. Values of $(\langle \mathrm{ADC} \rangle / \sigma_{\mathrm{ph}})^2$ measured for different scintillator materials at various beam positions along the counter.

The short transition time spread photomultiplier R1828-01 from Hamamatsu has been considered as optimum candidate, and compared to other possible choices in terms of time resolution and rate capability, as described next.

3.2.1. Time resolution

Three identical scintillator counters were equipped with the photomultipliers indicated in Table 2, and studied in a beam test at CERN. The first two photomultipliers are based on a 12-dynode linear focused structure, whereas the third one (R2490) uses a fine mesh electrode structure with 16 amplification stages, specially made for good time resolution performance [8]. Each counter was connected to two photomultipliers, one at each end.

The delay between the external trigger signal and the signal from each photomultiplier was digitized by a C414 CAMAC TDC, using a C808 constant fraction discriminator. To avoid the jitter of the trigger signal, the time differences $t_1 - t_2$ between both ends were off-line analysed. Considering that the timing features of both photomultipliers are the same, we can obtain the time

Table 2
Features of the three photomultipliers tested, according to the manufacturers [8,9]. They include rise time, transition time, transition time spread, number/type of dynodes and radiant photocathode sensitivity. The latter values are quoted at the wavelength corresponding to the maximum sensitivity (~420 nm in all cases)

PMT	Rise time (ns)	TT (ns)	TTS (ns)	Multiplication section	Ph. C. Sensitivity (mA/W)
R1828-01	1.3	28	0.231	12/Linear	85
XP2020	1.5	36	~ 0.250	12/Linear	80
R2490	2.7	14	0.150	16/Mesh	70

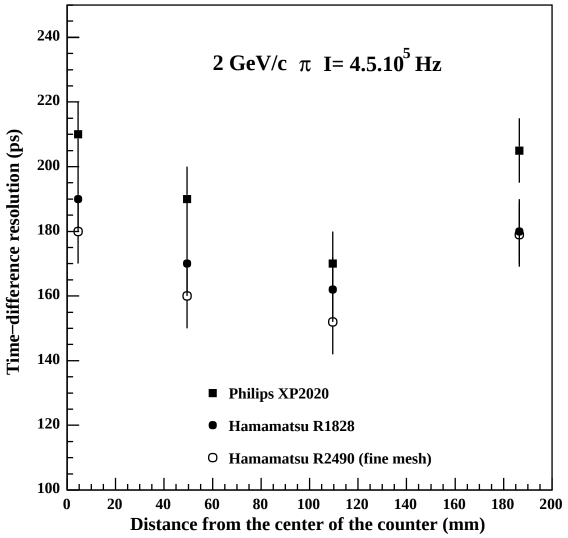

Fig. 5. Time resolution obtained in the beam-test with the photomultipliers indicated in Table 2. The results are shown for several beam positions along the counter.

resolution for a single measurement by dividing the sigma value of this distributions by the square root of two:

$$\sigma_T = \frac{\sigma_{t_1-t_2}}{\sqrt{2}} = \frac{\sigma_{\Delta T}}{\sqrt{2}}. \tag{2}$$

In Fig. 5, the resolution in the time difference ($\sigma_{\Delta T}$) is shown for the three prototypes, at several beam positions along the counter. In all cases, the average time resolution is better than the required 200 ps. Because the resolution values are systematically lower for the Hamamatsu photomultipliers R1828 and R2490 than for the Philips XP2020, we only retained the former two for further tests on the rate capability, as described in the following section.

3.2.2. Rate capability

In the high particle flux of the DIRAC experiment the design of the voltage divider is critical, because the bleeder circuit defines the rate limit for linear operation.

We want to keep the photomultiplier gain stable against the incoming particle flux, within a safe operation range up to 1 MHz. This implies a linear operation in the detector, i.e. proportionality between the anode current (I_a) and the incident flux in the photocathode. Non-linearity effects appear when, due to high rate operation, I_a increases in such a way that the voltage drop in the last amplification stages becomes significant and causes gain instability, due to insufficient bleeder current (I_c) supply.

The relative variation of the gain is proportional to the ratio between anode and bleeder current [10]. For a large number n of amplification stages ($n = 12$, in our case), and moderately large value of the secondary emission factor ($\delta \approx 4$), it can be approximated by the expression:

$$\frac{\Delta G}{G} \approx \frac{n}{n+1}\frac{I_a}{I_c}. \tag{3}$$

In order to evaluate this effect and with the aim of determining the rate capability of our prototypes, a laboratory test was performed. A red LED source connected to a pulse generator was used to simulate an increasing particle rate. The light output was set to generate a signal approximately equal to the one produced by a MIP, and delivered at the center of the counter. Amplitude and width of the photomultiplier output signal where studied as function of the LED frequency.

The results obtained using the R1828 photomultiplier equipped with the standard voltage divider designed by Hamamatsu are shown in

Fig. 6 (open circles). When the frequency is increased the amplitude and width remain constant up to a maximum value $\sim 1 \times 10^3$ Hz where they abruptly change. This signal saturation will certainly affect the time resolution, and it is well below the DIRAC specifications. Note that this behavior is related with the voltage drop in the last amplification stage, as indicated in the bottom part of Fig. 6.

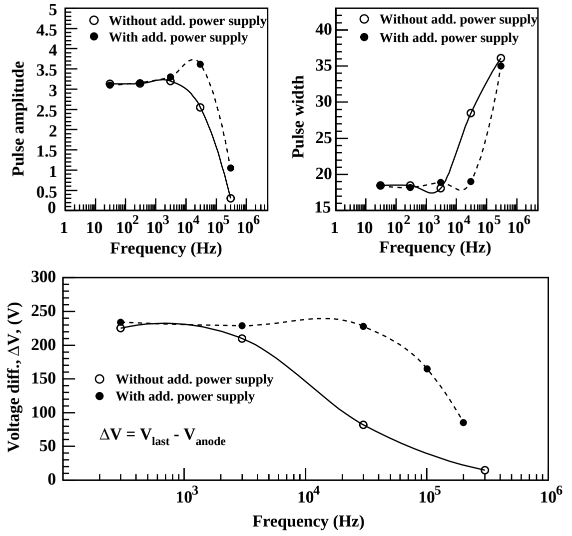

Fig. 6. Dependence of pulse amplitude (top left) and pulse width (top right) of the signal as function of the LED frequency. Variation of the voltage drop through the last amplification stage (bottom). The effect of providing an additional power supply can be also appreciated.

A common solution to increase the rate capability of such a scintillation detector is to use an additional power supply in the last dynodes (booster), to allow an increased bleeder current. This was done and the result shows some improvement Fig. 6 (black circles) with a measured current of 2 mA, but the rate capability is still insufficient. A new bleeder circuit was then designed (see Fig. 7) to increase the current through the divider by a factor ~ 3. We compared the performance of this divider (referred to as DIRAC circuit) with that of the standard divider, boosted by either one or two additional power supplies. A maximum acceptable rate was defined in each case according to the LED tests illustrated in Fig. 6, particularly from the width increase. The performance of the R2490 photomultiplier from Hamamatsu (with standard divider) was also included in the comparison for reference. The results for the maximum frequency achieved in each case are shown in Fig. 8(a). It is observed that 2 MHz can be reached with our voltage divider, with the R1828 photomultiplier. This determined our choice, given the fact that the high performance R2490 (see Fig. 5), is less cost-effective.

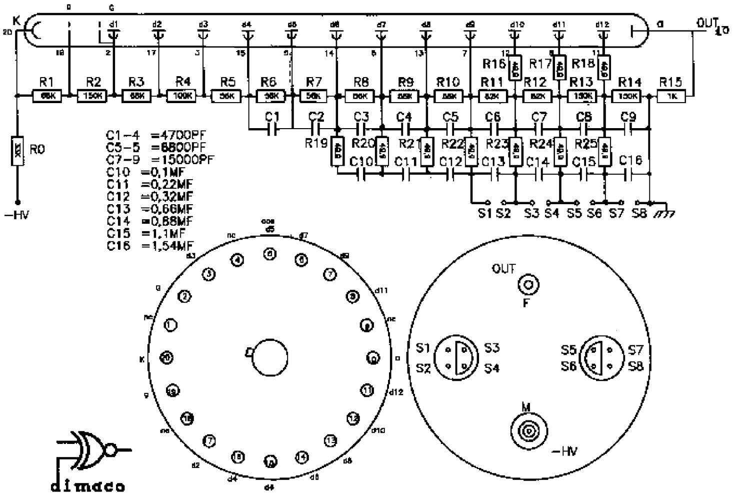

Fig. 7. Voltage divider for the R1828-01 photomultiplier optimized for DIRAC operation.

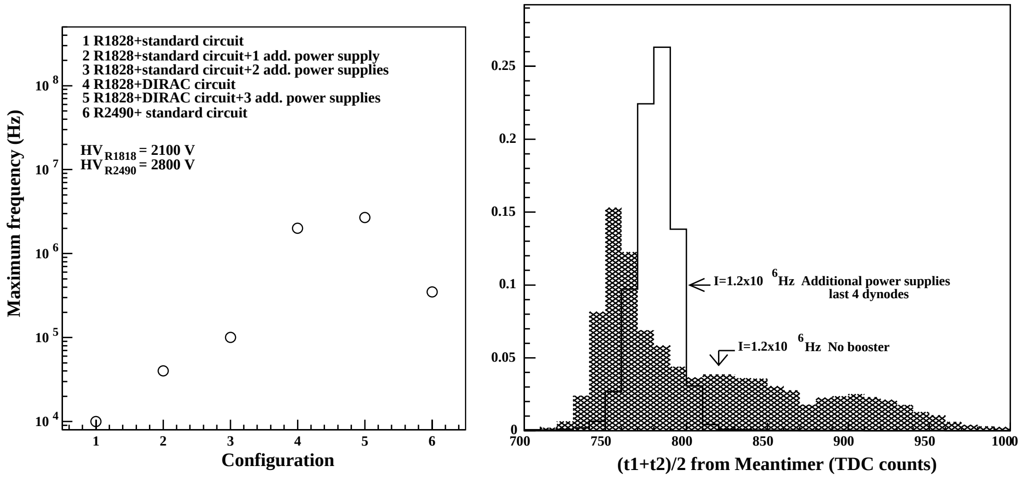

Fig. 8. Maximum operation frequency obtained from LED tests for the photomultiplier and voltage divider configurations indicated in the figure onset, as described in the text (left). Time distributions obtained for the R1828-01 equipped with the DIRAC voltage divider, with and without additional power supply (right).

Further tests on rate capability were performed with the pion beam at CERN, using the electronics previously described. We show in Fig. 8(b) the shape of the $(t_1 + t_2)/2$ distribution from the meantimer output (in TDC counts) at 1.2 MHz rate, using the R1828-1 photomultiplier equipped with the DIRAC divider. It becomes clear that without use of additional power supply, the signal is strongly distorted. But when the last 4 dynodes are powered independently, a prompt time distribution is restored.

3.3. Electronics readout

In order to minimize time slewing effects with signal amplitude and to achieve a time definition independent of particle impact point, we chose to use Constant Fraction Discrimination coupled with Mean Timers. We tested the LeCroy L3420 and the CAEN C808 constant fraction discriminators, both in conjunction with the CAEN C561 meantimer. In addition, a special unit developed in the Juelich Laboratory that integrated both concepts called RALEX [11], was included in the tests. Digitization of $(t_1 + t_2)/2$ values was achieved by means of a CAEN C414 TDC stopped by the meantimer output. At the CERN T9 pion beam, a comparison was made between the three different

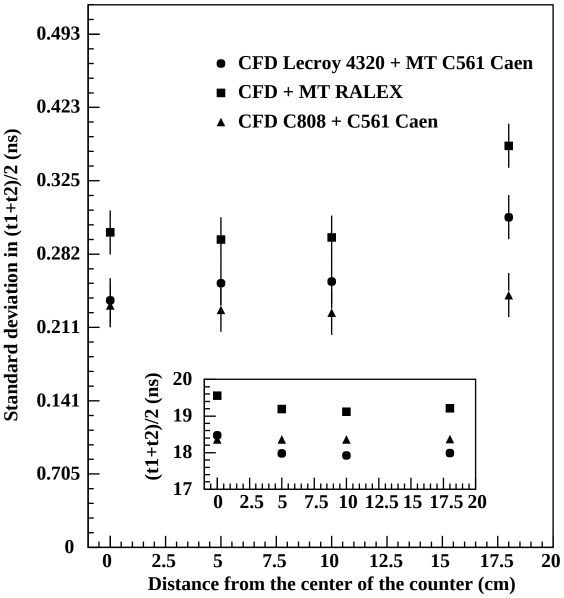

Fig. 9. Resolution in $(t_1 + t_2)/2$ for three different choices of the constant fraction discriminator and meantimer units, as indicated in the figure. The insert shows the variation of the average time as function of the beam incident position.

setup in terms of resolution and time uniformity as function of the beam position (measured from the center of the counter). The results are illustrated in Fig. 9 and show a good performance in all cases, with slightly better behaviour for the couple C808 and C561 in both resolution and uniformity.

4. DIRAC setup and performance

The detector was installed in the spectrometer in July 1998, and DIRAC has been collecting data since summer 1999. The geometrical layout of both telescope arms has been described in Section 3, and it is shown in Fig. 2. The photomultiplier signals are split to participate in the trigger (first and third level) and to be read out by the DAQ system. The latter must be delayed approximately 400 ns in order to await trigger decision. The delay line has been considered in some detail in order to preserve the time resolution. After several tests it was decided to use 79 m shielded twisted-pair cable, NK networks 9923, that provides a double pulse resolution of 60 ns with time jitter smaller than 80 ps.

Constant Fraction Discrimination is achieved by LeCroy L3420 units, followed by CAEN C561 Mean Timers to provide position independent timing. Time digitization is performed by a LeCroy L4303 Time to FERA Converter (TFC) followed by a L4300B-600 ADC. The combined resolution attained by this ensemble reaches 62 ps. We summarize next the main results concerning the detector performance.

4.1. Counting rates and detector efficiency

The measured particle rates in the vertical hodoscope system depend on background conditions, target choice and beam intensity. The first has been evaluated by making rate measurements with and without target, where a relation 20–1 has been achieved in the 2000 run. Fig. 10 shows the average rate (per arm and per spill) measured using the 95 μm Ni target for different values of the beam intensity, up to 8×10^{10} p/spill.

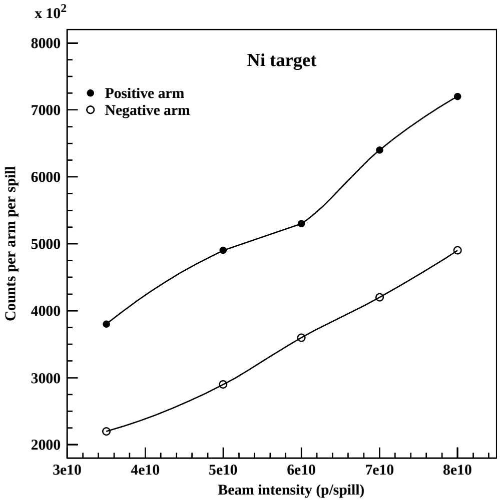

Fig. 10. Integrated rates as function of the proton beam intensity for the Ni target.

In Fig. 11 we show how these particles are distributed over the 36 counters, in the positive (a) and negative (b) arms, for a beam intensity up to 8×10^{10} p/spill. The measured rates scale approximately linear with intensity within the tested values up to 1×10^{11} p/spill. When proper normalization to the observed total rate is done, the profiles shown in Fig. 11 appear to be unchanged as function of beam intensity. There are thus no losses due to saturation effects in the indicated intensity range. Counter numbering for the positive arm runs from 1 to 18, moving from the outer part towards the beam. For the negative arm, it runs from 19 to 36 again from outside to inside.

Detector efficiency has been evaluated using the information from the drift chambers and the horizontal hodoscopes. Multiple track events were used, in order to avoid the trigger correlation. By extrapolating the particle tracks to the vertical hodoscope plane we determined the detector efficiency as function of the local coordinate. The overall detector efficiency is 98.6%, referred a continuous coverage of the solid angle. The main source of the inefficiency resulted to be geometrical, related to the dead spaces between counters (0.72% for the negative arm and 0.56% for the positive one). The intrinsic efficiency obtained was 99.9%.

4.2. Time resolution

As explained earlier, precision in the time difference between both arms is critical for the DIRAC experiment, in regard to both the

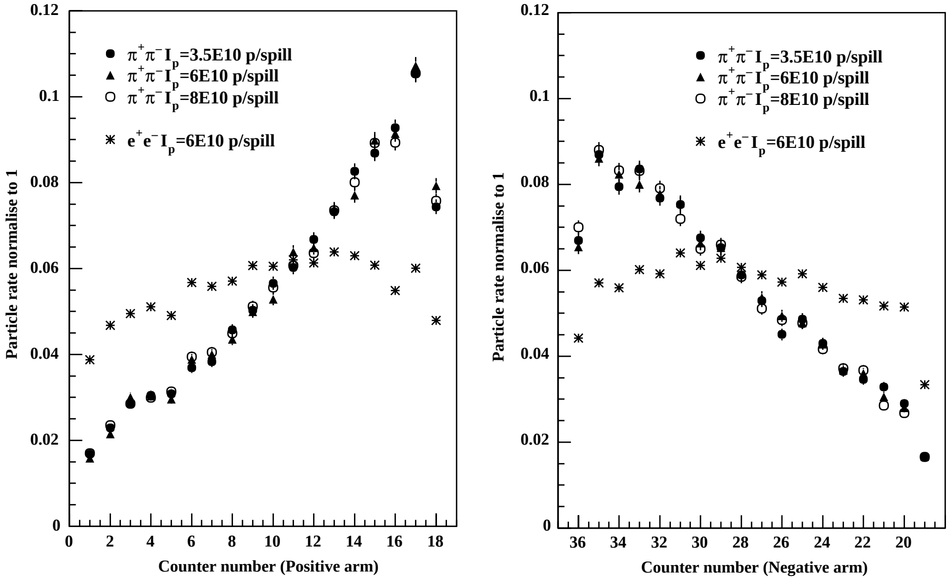

Fig. 11. Counting rates per counter obtained for pion triggers at beam intensities ranging from 3.5×10^{10} to 8×10^{10} p/spill, and for electron triggers at 6×10^{10} p/spill. The rates have been normalized to the total counting rate in each case, so that the histograms appear to have the same area.

separation of Coulomb-correlated pairs and the rejection of $p\pi^-$ and $K\pi$ background.

In order to determine and calibrate the detector time resolution we have used a high purity e^+e^- sample obtained with the DIRAC Cherenkov counters [12], normally used in anti-coincidence in the experiment [3]. This trigger mainly selects pairs from γ conversions and Dalitz pairs. Due to the ultra-relativistic kinematics of the electron in the momentum range $2<p<6$ GeV/c, the TOF for e^+e^- pairs does not depend on particle momentum. In addition, accidental coincidences for e^+e^- pairs within the 40 ns time window of the experiment are very rare, and practically all observed pairs are strongly time correlated.

Some cuts have been applied in order to make the analysis as close as possible to the one with pion pairs: only events with one counter hit in each arm, on both vertical and horizontal hodoscopes, have been considered. In addition, these events must have one reconstructed drift chamber track in each arm, and the timing measured in the vertical and horizontal hodoscopes are required to be compatible.

The data analysis requires in first place a time calibration (or time alignment) procedure, and secondly a correction to the time difference due to the different pathlength traveled by each particle in the pair. Time offsets between individual counter signals arise due to several reasons: small differences in photomultiplier performance (transit time), variations in the signal cable lengths, and channel-to-channel delays in the readout electronics. A 18×18 alignment matrix has been determined for all counter pairs, as main input for a calibration database.

The pathlength correction is calculated as follows: the hodoscope hit for a given particle is associated to a track segment measured in the drift chambers. Track bending is simulated by a kink at a point C, defined by the intersection of the segment extrapolation and a vertical plane perpendicular to the beam at the magnet center (see the overall layout in Fig. 1). The particle pathlength is then calculated as $L = L_1 + L_2$, where L_1 is the distance between the intersection point C and the hodoscope impact point, and L_2 is the distance between C and the beam center at the target position. The corrected time difference Δt_c is defined as

$$\Delta t_c = \Delta t - \frac{\Delta L}{c} \tag{4}$$

where ΔL is the difference in particle pathlengths as described before, and Δt is the difference between time-aligned measured values.

For simplicity, we have considered here only the combinations of symmetrical counters with respect to the detector center line, following the numbering convention illustrated in Fig. 11. The time resolution was obtained by means of a Gaussian fit for each combination, and it is shown in Fig. 12. We indicate separately the results obtained before and after the pathlength correction. It is clear that the improvement is significant, specially for the counters at larger angles. The observed resolution in the time difference is better than 200 ps for all combinations. Indeed, this correction causes the resolution values to be quite uniform across the detector, ranging from 150 to 200 ps.

We have also determined the global (average) resolution in the time difference Δt_c using the whole sample of e^+e^- events (with the cuts previously reported), including all counter combinations that actually happen in the spectrometer data. The Δt_c distribution is shown in Fig. 13. The sigma value obtained from a Gaussian fit is 174 ps. From this result we quote an average time resolution per counter of 123 ps, according to expression (2).

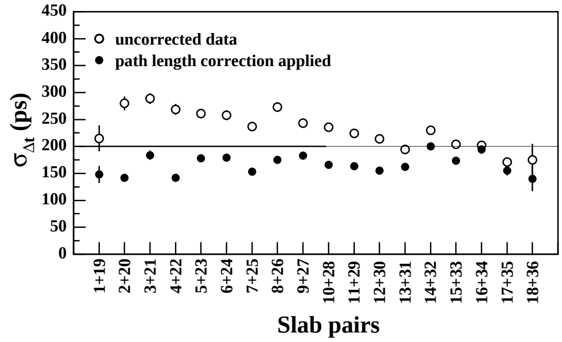

Fig. 12. Resolution in the time difference measured with e^+e^-, for each symmetrical pairs of counters. The results are shown before and after the pathlength correction.

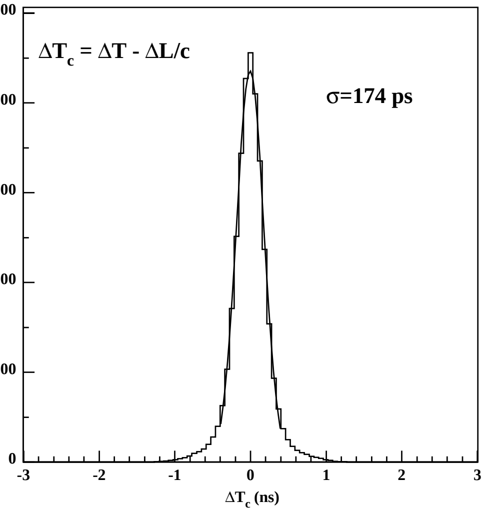

Fig. 13. Average time resolution determined with e^+e^- pairs, including the pathlength correction.

In Table 3 we summarize the main design and geometrical features of TOF detectors found in the literature [5] for different particle physics experiments, including their published values of the time resolution. Clearly, the DIRAC detector is among the most accurate.

5. Separation of real and accidental hadron pairs

The extrapolation method proposed in DIRAC [1] to determine the pionium lifetime requires a precise knowledge of the relative $\pi^+\pi^-$ momentum spectra for both the time correlated pairs (which we call real pairs) and uncorrelated (accidental) pairs.

Contrary to the electron case, the pion velocity is a function of the momentum that needs to be taken into account, if we want to have a precise determination of the actual time difference between the two particles at production time. Making the pion mass hypothesis, and using the particle momentum and trajectory measured by the DIRAC spectrometer, we calculate the predicted difference in arrival time to the hodoscopes as

$$\Delta t_{\text{pred}} = \frac{L_+}{c}\sqrt{1 + \left(\frac{m_+}{p_+}\right)^2} - \frac{L_-}{c}\sqrt{1 + \left(\frac{m_-}{p_-}\right)^2} \tag{5}$$

Table 3
Comparison of time resolution for several TOF detectors

Detector	Scintillator	Length (cm)	Width (cm)	Thickness (cm)	Photomultiplier	σ (ps)
CERN [13]	NE102A	25	8	2	Phi. XP2020	123
DASP [14]	NE110	172	20	2	RCA 8575	210
E813 [15]	BC408	200	8.5	5	Ham. H1949	110
ARGUS [16]	NE110	218	9.3	2	RCA 8575	~ 210
CLEO II [17]	BC408	280	10	5	Amp. XP2020	139
OBELIX [18]	NE110	300	~ 9.3	4	Phi. XP2020	170
E735 [19]	BC408	305	10	5	Phi. XP2020	110
MARK III [20]	NE Pilot F	317.5	15.6	5.1	Amp. XP2020	~ 171
DELPHI [21]	NE110	350	20	2	EMI 9902KB	1200
CLAS [22]	BC408	32–450	15–22	5.1	XP4312B/D1	163
DIRAC	BC420	40	7	2.2	Ham. R1828-01	123

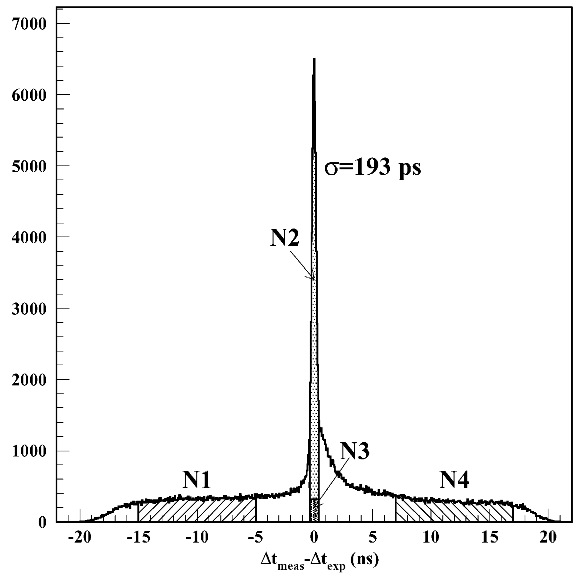

Fig. 14. Time difference between positive and negative particles with the standard hadron trigger, after the pion velocity correction.

where L_{+-}, p_{+-} and m_{+-} are the particle path-lengths, momenta and mass, respectively, for positive and negative particles. It is assumed that $m_+ = m_- = m_\pi$. So we determine the difference between the measured time interval (after time alignment) Δt_{meas} and the predicted one: $\Delta t = \Delta t_{\mathrm{meas}} - \Delta t_{\mathrm{pred}}$. This distribution is shown in Fig. 14 for a hadron sample obtained with the standard DIRAC $\pi^+\pi^-$ trigger. A narrow peak is observed which corresponds to the real (Coulomb correlated) pairs ($N2 + N3$ in Fig. 14), and a flat background of accidental pairs ($N1 + N4$ in the same figure) mostly originated by hadrons that belong to different proton–nucleus interactions. The excess in the right-hand wing of the peak is due to contamination of final state protons from target fragmentation (see later). The sigma value obtained by making a Gaussian fit to the peak (193 ps) is similar to that achieved for the e^+e^- sample, as reported previously. The time spectrum shown in Fig. 14 is used in the experiment to perform off-line separation between real and accidental pairs, thus allowing a precision calibration of the Coulomb interaction.

6. Identification of pπ- and Kπ pairs

Fig. 15 (top) shows the momentum spectrum measured by the spectrometer in the laboratory system for positive and negative particles, selected by the standard hadron trigger. It covers the interval between 1.5 GeV/c and 7 GeV/c. In the bottom part of Fig. 15 we show how this momentum spectrum correlates with the TOF counter numbers in each arm. As expected from the detector segmentation in the bending plane, high momentum is seen by the counters closer to the beam.

The pπ^- identification is clearly appreciated in the correlation between the time difference measured in the TOF detector (with pion velocity correction) and the particle momentum, which is represented in Fig. 16. Two bands are clearly observed over the background of accidental pairs. The vertical one, centered around zero, shows the $\pi^+\pi^-$ signal (with a possible component of other equal mass pairs). The second band represents $p\pi^-$ pairs, where the proton is slowed down due to its higher mass. Also shown in the insert of Fig. 16 is the kinematic prediction of this curve, which agrees well with the data. The experimental points represent the results of a Gaussian fit to the peak value of Δt in different momentum bins. A similar fit procedure also shows a small signal for $K\pi$ pairs. Another way to present these results is to plot the distribution of the positive particle mass according to expression (5), once the pion mass has been fixed for the negative one. The result is shown in Fig. 17, where the proton and kaon peaks are clearly visible.

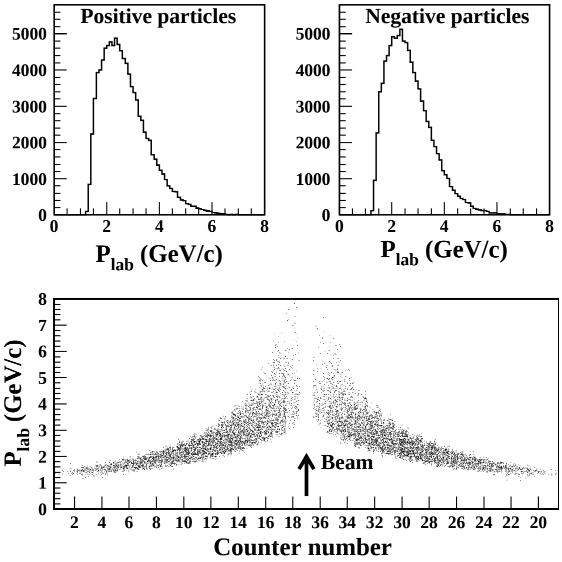

Fig. 15. Momentum spectra in the laboratory system for positive (top left) and negative (top right) particles, selected by the standard hadron trigger. Correlation between the particle momentum and the counter number (bottom). The beam position is indicated for reference.

7. Summary

A time-of-flight detector array has been built and it is operational for the DIRAC experiment at CERN with 123 ps average resolution for all counters. This resolution is uniform across the detector acceptance and it has been tested with particle rates up to 1 MHz per counter.

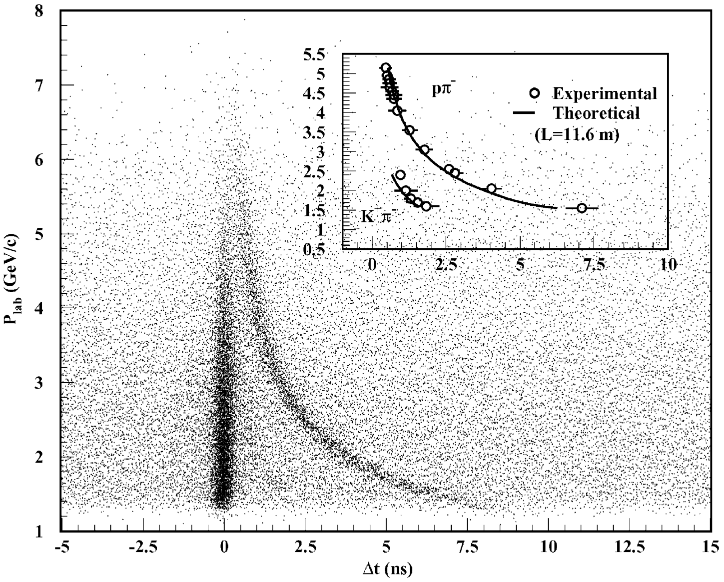

Fig. 16. Correlation between the time difference measured, after pion velocity correction, and the particle momentum measured by the spectrometer in the laboratory frame.

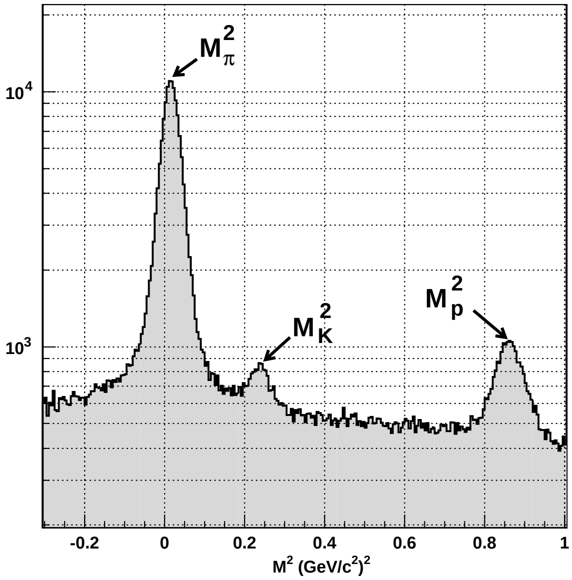

Fig. 17. Distribution of the positive particle mass, according to expression (5), for particle pairs selected with the standard hadron trigger. The negative particle mass has been set to m_π.

Acknowledgements

The group would like to acknowledge the invaluable help and advice received from Rykaline and L. Nemenov in many discussions about the general performance of the detector in the experiment. We also thank A. Koulikov and V. Brekhovskikh for their help in detector operation at CERN, V. Karpukhin for his advice on the issue of cable transmission, and V. Komarov for his contribution to the detector support structure.

References

[1] B. Adeva, et al., CERN/SPSLC 95-1 SPSLC/P 284 (1994).
[2] B. Adeva, et al., DIRAC: a high resolution spectrometer for Pionium detection, Nucl. Instr. and Meth., to be published.
[3] L. Afanasyev, et al., The multilevel trigger system of the DIRAC experiment, Nucl. Inst. and Meth. A, to be published, hep-ex/0202045; see also L. Afanasyev, M. Gallas, V. Karpukhin, A. Kulikov, Nucl. Inst. and Meth. A 479 (2002) 407.
[4] M. Gallas, The complete software-programmable third level trigger for DIRAC, Application Note AN-60, LeCroy Corporation, 1999.
[5] E.S. Smith, et al., Nucl. Instr. and Meth. A 432 (1999) 265.
[6] V. Rykaline, private communication, 1996.
[7] A.M. Rodríguez, Ph.D. Thesis, Santiago de Compostela, 2000.
[8] Hamamatsu Photonics K.K., Electron Tube Center, Technical Data, October 1992.
[9] Data Handbook Photomultipliers, Philips Book PC04, 1990.
[10] W.R. Leo, Techniques for Nuclear and Particle Physics Experiments, 2nd Revised Edition, Springer, Berlin, 1994.
[11] R. Schleichert, A. Selikov, H. Seyfarth, Development of a constant fraction discriminator and meantimer, IKP Annual Report 1995, Forschungszentrum Juelich, 1996, pp. 65–66.
[12] M. Bragadireanu, et al., Nucl. Inst. and Meth. 426 (1999) 254.
[13] F. Binon, et al., Nucl. Instr. and Meth. 153 (1978) 409.
[14] W. Braunschweig, et al. (DASP Collaboration), Nucl. Instr. and Meth. 134 (1976) 261.
[15] V. Sum, et al. (E813 Collaboration), Nucl. Instr. and Meth. A 326 (1993) 489.
[16] R. Heller, et al. (ARGUS Collaboration), Nucl. Instr. and Meth. A 235 (1985) 26.
[17] Y. Kubota, et al. (CLEO II Collaboration), Nucl. Instr. and Meth. A 320 (1992) 66.
[18] G.C. Bonazzola, et al. (OBELIX Collaboration), Nucl. Instr. and Meth. A 356 (1995) 270.
[19] S. Banerjee, et al. (E735 Collaboration), Nucl. Instr. and Meth. A 269 (1988) 121.
[20] J.S. Brown, et al. (MARK III Collaboration), Nucl. Instr. and Meth. 221 (1984) 503.
[21] J.M. Benlloch, et al. (DELPHI Collaboration), Nucl. Instr. and Meth. A 292 (1990) 319.
[22] J.M. Benlloch, et al., Nucl. Instr. and Meth. A 290 (1990) 327.